ARTICLE

Cu₂Se and Cu Nanocrystals as Local Sources of Copper in Thermally Activated *In Situ* Cation Exchange

Alberto Casu,[†,‡,△] Alessandro Genovese,[†,‡,△] Liberato Manna,[*,†] Paolo Longo,[⊥] Joka Buha,[†] Gianluigi A. Botton,[∥] Sorin Lazar,[∥,¶] Mousumi Upadhyay Kahaly,[§] Udo Schwingenschloegl,[§] Mirko Prato,[†] Hongbo Li,[†,#] Sandeep Ghosh,[†] Francisco Palazon,[†] Francesco De Donato,[†] Sergio Lentijo Mozo,[‡] Efisio Zuddas,[‡] and Andrea Falqui[*,‡]

[†]Department of Nanochemistry, Istituto Italiano di Tecnologia, Via Morego 30, 16163 Genova, Italy

[‡]NABLA Lab, Biological and Environmental Sciences and Engineering (BESE) Division and [§]Physical Sciences and Engineering (PSE) Division, King Abdullah University for Science and Technology (KAUST), Thuwal 23955-6900, Kingdom of Saudi Arabia

[⊥]Gatan, Inc., 5794 W Las Positas Boulevard, Pleasanton, California 94588, United States

[∥]Department of Materials Science and Engineering, McMaster University, Hamilton, Ontario L8S 4L8, Canada

[¶]FEI Electron Optics, Achtseweg Noord 5, Eindhoven 5600 KA, The Netherlands

[#]Chemistry Division, Los Alamos National Laboratory, Los Alamos, New Mexico 87545, United States

S *Supporting Information*

ABSTRACT: Among the different synthesis approaches to colloidal nanocrystals, a recently developed toolkit is represented by cation exchange reactions, where the use of template nanocrystals gives access to materials that would be hardly attainable *via* direct synthesis. Besides, postsynthetic treatments, such as thermally activated solid-state reactions, represent a further flourishing route to promote finely controlled cation exchange. Here, we report that, upon *in situ* heating in a transmission electron microscope, Cu₂Se or Cu nanocrystals deposited on an amorphous solid substrate undergo partial loss of Cu atoms, which are then engaged in local cation exchange reactions with Cu "acceptor" phases represented by rod- and wire-shaped CdSe nanocrystals. This thermal treatment slowly transforms the initial CdSe nanocrystals into Cu₂₋ₓSe nanocrystals, through the complete sublimation of Cd and the partial sublimation of Se atoms. Both Cu "donor" and "acceptor" particles were not always in direct contact with each other; hence, the gradual transfer of Cu species from Cu₂Se or metallic Cu to CdSe nanocrystals was mediated by the substrate and depended on the distance between the donor and acceptor nanostructures. Differently from what happens in the comparably faster cation exchange reactions performed in liquid solution, this study shows that slow cation exchange reactions can be performed at the solid state and helps to shed light on the intermediate steps involved in such reactions.
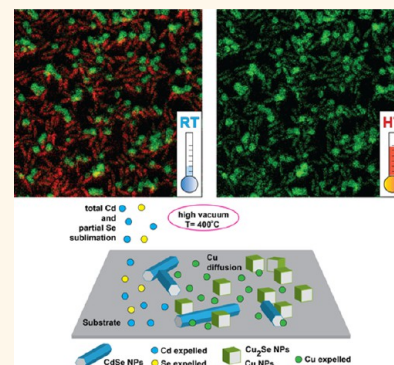
KEYWORDS: *in situ transmission electron microscopy, cation exchange, scanning transmission electron microscopy, energy-dispersive X-ray spectroscopy, electron energy loss spectroscopy, energy-filtered transmission electron microscopy*

Cation exchange (CE) reactions[1,2] in ionic crystals involve the partial or the complete replacement of the cation sublattice, while the anion sublattice remains in place and is essentially preserved in the transformation,[3−6] giving access to materials that would be otherwise difficult to synthesize through a direct synthesis.[7−9] This kind of process is generally based on the fast direct reactions between inorganic colloidal nanocrystals (NCs) and cationic species, both dispersed in the same liquid phase. In such a system, the very dynamic nature of the reaction environment makes direct

monitoring of the process very difficult and, at present, certainly not suitable to single-particle tracking with high spatial resolution. Classical NC systems on which CE reactions have been tested extensively belong to copper chalcogenides and to the II−VI and IV−VI classes of semiconductors.[3−6] Copper chalcogenides are particularly prone to CE reactions because in
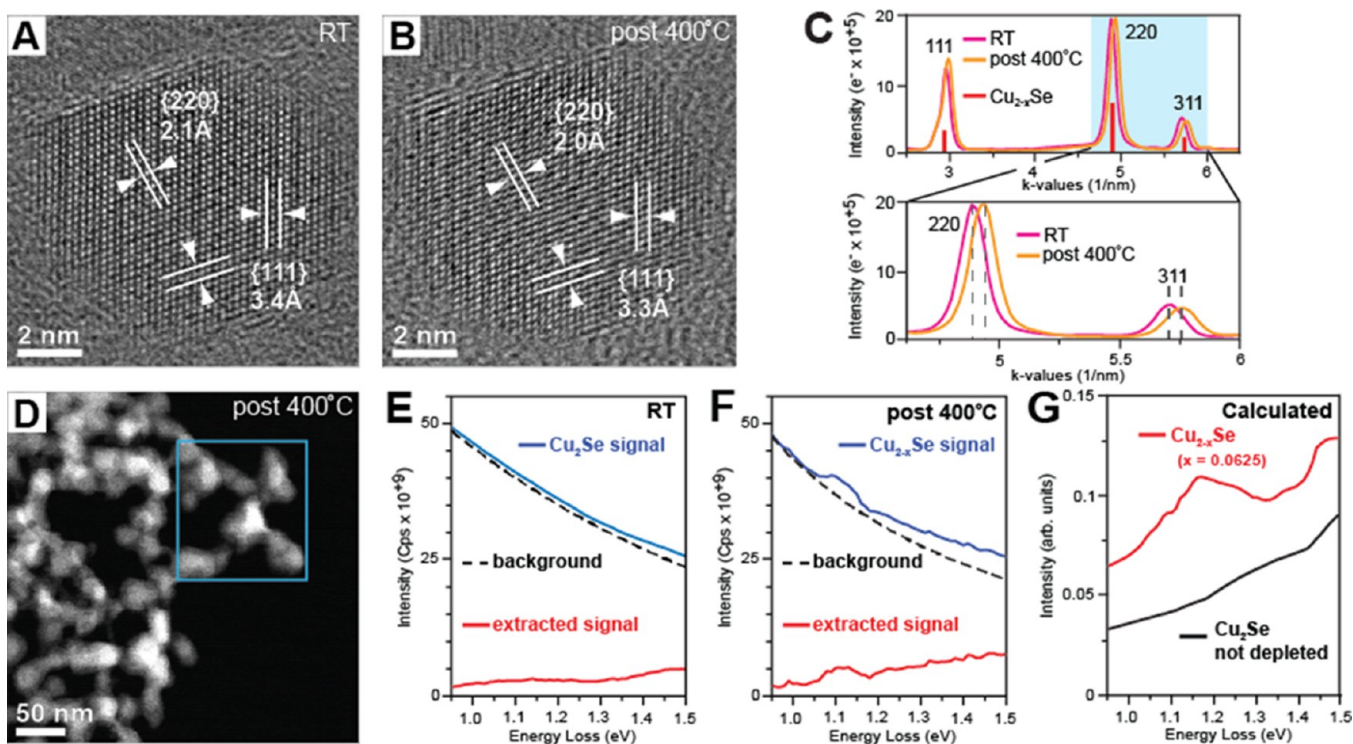
Figure 1. HRTEM, ED characterization, STEM, HR-EELS, and EELS simulation of cubic Cu_2Se NCs before and after thermal treatment at 400 °C. (A,B) HRTEM details of a single Cu_2Se NC, observed along its $[1\bar{1}0]$ zone axis, before (RT) and after (post 400 °C) thermal treatment and exhibiting a small decrease in d spacings, consistent with the slight lattice shrinkage due to Cu loss. (C) Comparison between integrated linear profiles of ED patterns at RT (magenta) and post-thermal treatment at 400 °C (orange), indexed according to cubic $Cu_{2-x}Se$ structure. The slight shift of diffraction peaks toward higher k values confirms the small shrinkage of the lattice due to Cu loss. Inset: Detail of (220) and (311) diffraction peaks with their corresponding shift, as observed after the thermal treatment. (D) STEM imaging of $Cu_{2-x}Se$ NCs after thermal treatment, showing the region with $Cu_{2-x}Se$ NCs investigated by HR-EELS (blue square). (E) HR-EELS spectrum of Cu_2Se NCs, from which no remarkable feature was seen in the low loss energy region. (F) HR-EELS spectrum of $Cu_{2-x}Se$ NCs, which instead shows a peak at 1.1 eV in the low loss energy range (from 0.95 to 1.35 eV), correlated to a localized surface plasmon absorption due to the collective excitation of holes (arising from the presence of Cu vacancies) in the valence band of $Cu_{2-x}Se$. (G) DFT simulation of HR-EEL spectrum in the low loss region of $Cu_{2-x}Se$ NCs, evidencing the presence of a feature at 1.1 eV in the same energy range of 0.95–1.35 eV, which is instead absent in a NC of stoichiometric Cu_2Se.

these materials the formation of a large number of Cu vacancies provides efficient pathways for cation interdiffusion and exchange.[10] Bekenstein *et al.* recently showed that the thermal annealing of a film of copper sulfide NCs increased the number of Cu vacancies in the NCs, resulting in a modification of their electronic properties.[11] Similarly, different groups investigated the variation in the optical behavior of copper chalcogenide NCs when subject to postsynthetic processes which modify the Cu stoichiometry, demonstrating a direct correlation between Cu deficiency (x) in the NC lattice and the emergence of a localized surface plasmon resonance (LSPR).[12−14] Copper chalcogenides have the additional peculiarity of undergoing a phase transition above a thermal threshold to a superionic (SI) phase, with highly mobile copper ions in the lattice.[15−20] In particular, copper selenide (Cu_2Se) transforms at high temperature into a Cu-depleted superionic $Cu_{2-x}Se$ phase, characterized by a liquid-like behavior of the Cu cations within a rigid Se sublattice having face-centered cubic (fcc) structure.[18−20] Here, we aimed to assess whether Cu_2Se NCs do lose a measurable fraction of Cu atoms from their lattice once deposited on a substrate and annealed above a certain threshold temperature. If so, our next goal was to clarify if the expelled Cu species could engage in "dry" CE reactions, involving NCs of another ionic material deposited on the same substrate, in our case either CdSe nanorods (NRs) or CdSe

nanowires (NWs). To perform this study, we made extensive use of state-of-the-art *in situ* transmission electron microscopy (TEM) and related spectroscopic techniques. By these means, we were able to both trigger the CE process and follow it with the highest spatial and temporal resolution.

RESULTS AND DISCUSSION

***In Situ* TEM Annealing of sole Cu_2Se Nanocrystals.** As a starting experiment, colloidally synthesized Cu_2Se NCs were placed on a TEM carbon-coated grid. Using a TEM heating holder, careful morphostructural and chemical analyses of the NCs were performed at room temperature (RT), before and after *in situ* heating. Such a heating step consisted of keeping the holder at a target temperature for a given time. We found a threshold temperature of 400 °C and a heating time of about 60 min as parameters for a detectable Cu depletion in the NCs. High-resolution TEM (HRTEM) of individual NCs and electron diffraction (ED) analysis on groups of NCs (after annealing, in order to avoid any lattice thermal expansion effect) indicated that, while the cubic structure of the initial NCs was preserved, their lattice had slightly contracted (Figure 1A,B). In particular, linear integrated ED profiles displayed a slight shift of the diffraction peaks toward higher nm^{-1} values, in the reciprocal space, with respect to the nonannealed NCs (Figure 1C). The main (220) diffraction peak shifted from
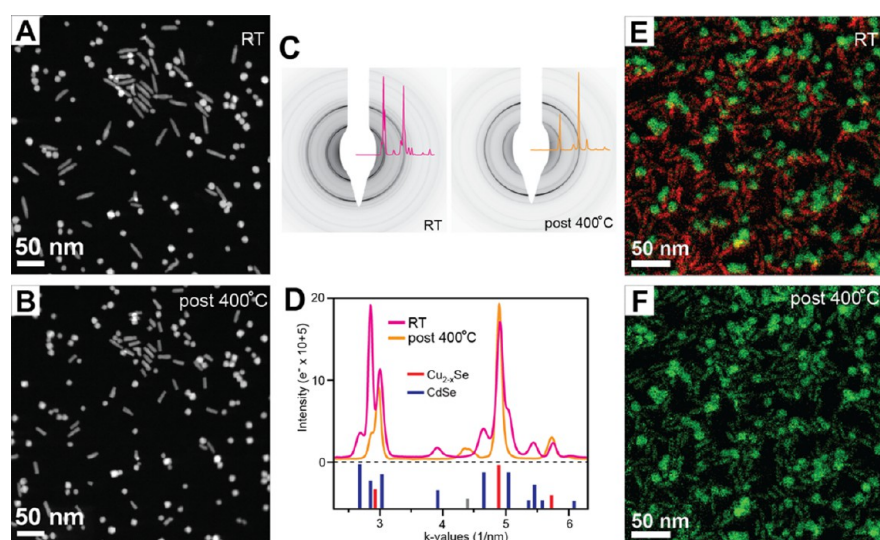
Figure 2. STEM, electron diffraction, and energy-filtered TEM characterization of Cu₂Se and CdSe NCs at pre- and post-heating stages. (A,B) HAADF-STEM images of a representative region featuring the different phases at RT and after the annealing at 400 °C, respectively. (C) Selected area electron diffraction patterns of a representative region featuring Cu₂Se NCs and CdSe nanorods at RT and post-thermal treatment at 400 °C with superposition of the 1D profile of the ED signal, as obtained by integration over the full round angle in the reciprocal space. (D) Comparison between integrated linear profiles of ED patterns collected at RT pre- (magenta) and post-400 °C treatment (orange), revealing that the phase transformation occurred on the CdSe nanorod's component of the original mixture: the RT electron diffraction profile is indexed as a mixture of cubic antifluorite Cu₂Se and wurtzite CdSe, while after 400 °C treatment, only the cubic Cu₂₋ₓSe phase is found. The weak and broad peak at about 4.4 nm⁻¹ could be ascribable to a Cu₂Se compound with monoclinic structure.[28] (E) Normalized energy-filtered TEM mapping acquired at RT and revealing clearly Cu (green) and Cd (red) localization in the Cu₂Se and CdSe NCs, respectively. (F) Normalized energy-filtered TEM mapping acquired at 400 °C and revealing that the exchange in the nanorods occurred between Cu (green) and Cd (red).

4.868 to 4.921 nm⁻¹, indicating a decrease of about 3% of the unit cell volume that can be ascribed to a partial loss of Cu (see the Supporting Information for further details). These data were corroborated by chemical quantification via high-resolution electron energy loss spectroscopy (HR-EELS) using a monochromated scanning TEM (STEM) of several NCs (Figure 1D), which indicated a decrease in the Cu/Se atomic ratio from 2.01:1 of the pristine NCs to 1.91:1 in the annealed NC (Figure S1). Furthermore, HR-EELS analysis of the same Cu₁.₉₁Se NCs points to a change in the electronic band structure due to Cu depletion suffered by the crystal lattice: while in the low loss region of the Cu₂Se NCs no feature was detected (Figure 1E), an additional feature appeared in the same region at 1.1 eV of the EELS spectrum as a consequence of the copper depletion, as shown in Figure 1F,G and Figure S2. This was previously interpreted as directly correlated to a near-infrared absorption band in the range from 900 to 1600 nm and arising from a LSPR due to the presence of Cu vacancies.[12−14,21]

HR-EEL Spectrum's Density Functional Theory Simulations of the Cu₂Se Nanocrystals after Annealing. To further confirm that the feature observed in the low loss EEL spectrum at 1.1 eV was due to copper depletion, we modeled a HR-EEL spectrum of a Cu₂₋ₓSe finite crystal via density functional theory (DFT) calculations using the random phase approximation (see Materials and Methods for further details). The modeled EEL spectrum (Figure 1G) was in good agreement with the experimental data, providing ample support to the influence of the loss of Cu atoms on the electronic band structure of the NCs.

In Situ TEM Simultaneous Heating of Cu₂Se Nanocrystals and CdSe Nanorods. A second set of experiments was then aimed at assessing if the expelled Cu species could

activate CE reactions of other nanostructures equally arranged on the same substrate. The natural choice fell on CdSe, as NCs of this material have been shown to undergo rapid CE in solution even at RT.[3] In this case, spherical Cu₂Se NCs (whose transformation upon annealing was reported in the first paragraph) were deposited on the TEM grid's carbon film together with CdSe NRs. The different morphologies of NCs made their two populations easily distinguishable, as shown by the high-angle annular dark-field scanning TEM (HAADF-STEM) image reported in Figure 2A,B.

Before annealing, the sample was analyzed by mapping various regions of the grid in order to rule out any structural or compositional evolution taking place already at RT. Chemical analysis of single NCs, performed in STEM mode via energy-dispersive X-ray spectroscopy (STEM-EDX), yielded Cu₂Se and CdSe stoichiometries for the two types of nanostructures, respectively. Indexing of the linear integrated ED patterns, obtained from the same regions, confirmed the stable coexistence of both cubic antifluorite Cu₂Se and hexagonal wurtzite CdSe, as displayed in Figure 2C,D.

In the present work, each set of EFTEM maps recorded during the annealing experiments was treated according to an *a priori* noise-normalizing approach with the aim to minimize the human-based biasing effects, control the background, and improve the signal-to-noise ratio within the data set. Hence, this approach, once applied to the thermally sensitive Cu₂Se−CdSe system, allowed discriminating and comparing more clearly the faint signals of chemical species involved in CE reactions over time.[22] Normalized energy-filtered TEM (EFTEM) elemental mapping then proved the spatial localization of Cu and Cd in the two different types of NCs (Figure 2E). Annealing was performed using the same temperature ramps of the first experiment, and after 60 min at 400 °C, the
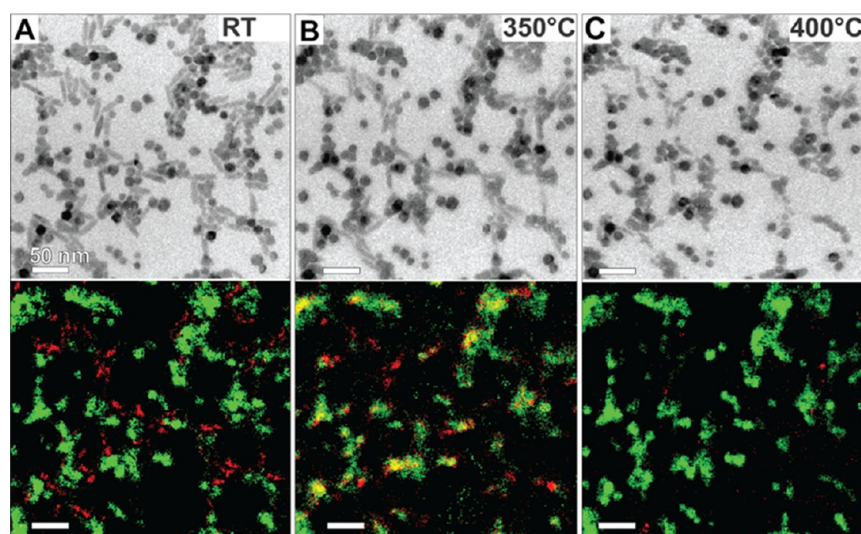
Figure 3. Sequences of normalized EFTEM elemental maps of Cu_2Se NCs and CdSe nanorods acquired at different temperatures. No CE reaction was observed between RT and 300 °C, with spatially distinct maps of Cd and Cu. At 350 °C, a partial superposition in the Cd and Cu maps indicates the beginning of CE reactions activated by the free Cu species, which randomly diffuses over the carbon film; note the dispersed Cu signal between the nanoparticles. After 30 min at 400 °C, the Cu CE reaction is completed. Color code: Cu, green; Cd, red; scale bars = 50 nm.

$Cu_{2-x}Se$ NCs exhibited a stable $Cu_{1.85}Se$ stoichiometry, revealing therefore a loss of Cu from their lattice. Moreover, Cd was no longer present in the rods, whose composition had become $Cu_{1.96}Se$, as assessed by STEM-EDX analysis. As no secondary nucleation of Cd-rich phases was observed on the carbon film, we concluded that the Cd species had sublimated under the high-temperature and vacuum conditions (see Table S2). Normalized EFTEM mapping confirmed the absence of Cd and the diffusion of Cu into the initial CdSe NCs (Figure 2F), while differences in intensity observed between $Cu_{1.85}Se$ NCs and $Cu_{1.96}Se$ nanorods should be attributed to the consistent differences in mean thicknesses of the two populations (*i.e.*, ~7 nm for the nanorods and ~12 nm for the NCs). Linear integrated ED pattern profiles of ensembles of NCs were indexed according to the cubic $Cu_{1.85}Se$ phase alone, denoting the complete transformation of the initial hexagonal wurtzite CdSe phase (Figure 2C,D). Annealing caused shrinkage in volume of both the Cu_2Se and CdSe NCs. However, while the $Cu_{1.85}Se$ NCs suffered only a small variation in average diameter, the starting CdSe NRs underwent a remarkable decrease in their mean length, from 34.8 to 21.9 nm, and a minor decrease in diameter, from 7.6 to 7.2 nm (Figure 2B). This corresponded to an average decrease in rods volume of 44%, estimated by approximating their shape to that of small cylinders, well above the theoretically volume contraction (12%) expected in going from wurtzite CdSe to antifluorite Cu_2Se, if a complete preservation of the Se anions would be assumed. Therefore, during the Cd → Cu CE reaction, part of the Se sublattice of CdSe sublimated, causing an additional volume loss of 36%, and that could be ascribed to concomitant causes, as discussed in the following. First, the binding energy of atoms on the apical facets is generally lower than that of the atoms inside the crystal lattice. This aspect, along with the change of crystal potential, due to cationic substitution and structural transition at high temperature, may promote the partial Se sublimation from the tips of NRs under the high-vacuum conditions of the TEM, also taking into account the very high vapor pressure of both Cd and Se, which

moreover scales with the temperature, as reported in Table S2 of the Supporting Information. Second, this occurrence should be also attributed to the case-to-case availability of Cu_2Se NCs acting as Cu donors for the CdSe nanorods. Once the threshold temperature for CE has been crossed and the CE reaction has started, if the quantity of locally available depleted Cu is not sufficient for a complete Cd-to-Cu substitution, a partial sublimation of Se from the anionic sublattice is triggered in order to preserve the electroneutrality of the nanorod structure. Similarly to the case of the Cd species, we concluded that the depleted Se sublimated under the high-temperature and vacuum conditions. As reported in detail in the Supporting Information, this allowed us to roughly calculate the free energy variation $(\Delta_R G)$ of the corresponding overall reaction: this is negative $(-138.6 \times 10^3$ kJ) and indicates that the exchange is thermodynamically favored under the experimental conditions.

Notably, neither reshaping nor shrinkage was observed in CdSe NCs annealed under the same conditions but in the absence of Cu_2Se NCs, which supports our hypothesis that the sublimation of Cd from the CdSe NCs was triggered by Cu atoms and partially destabilized the Se atoms, too, as clearly shown in Figure S3.

The evolution in the composition of the CdSe nanorods during the annealing from RT to 400 °C was studied by normalized EFTEM mapping, and the relevant results are reported in Figure 3. Here, the normalized EFTEM maps displayed an incipient onset of the exchange reaction at 350 °C, with Cu substituting Cd in the nanorods, as confirmed by the yellow zones in the map, which indicate local superimposition of Cd and Cu maps. At this temperature, we expected the start of Cd and Se sublimation and the consequent volume shrinkage of NRs. At 400 °C, the conversion of the nanorods from CdSe to $Cu_{1.96}Se$ was complete, with almost complete sublimation of Cd.

HRTEM observations revealed that, upon CE, the hexagonal close-packed (hcp) sublattice of Se anions in the initial CdSe NCs was reorganized into a cubic (fcc) sublattice. The lattice transformation preserved the close-packing direction, namely,

$[0001]_{hcp}$ in the initial wurtzite CdSe and $[111]_{fcc}$ in the final antifluorite $Cu_{1.96}Se$ rods (Figure 4A−C). Moreover, by performing fast HRTEM analysis while annealing the sample, we could visualize (Figure 4D,E) a gradual modification of the CdSe crystal structure, already at 350 °C, with the formation of sequential extrinsic stacking faults along the initial $[0001]_{hcp}$ direction of the CdSe rods. The formation of these structural

defects therefore changed the local strain field at the nanoscale within the crystal lattice, as assessed *via* peak pairs analysis (PPA)[25] (see Materials and Methods) reported in Figure 4D,E. Here, the shear strain field in the right region of the nanorod was almost unchanged from 350 to 400 °C, as in this temperature range the rod was able to retain the wurtzite CdSe structure, while compressive shear zones (blue) were compatible with the occurrence of intrinsic planar stacking faults. Conversely, the shear strain field in the left region exhibited a significant increase combined with a growth of tensile shear zones (red and yellow) from 350 to 400 °C, as shown by the integrated shear strain line profiles. This might be correlated to the formation of pervasive extrinsic planar stacking faults, due to the transformation of the Se crystal sublattice from wurtzite CdSe to antifluorite $Cu_{2−x}Se$, namely, from the hexagonal ABABAB to the final cubic ABCABCAB close-packing, during Cu cation exchange and Cd sublimation reactions.

In Situ TEM Simultaneous Heating of Cu₂Se Nanocrystals and CdSe Nanowires.

We carried out additional experiments in which wurtzite CdSe NWs instead of rod-shaped NCs were used as Cu acceptors. They gave rise to the same CE reaction observed with the CdSe rods. In this direction, the normalized EFTEM maps acquired under different thermal conditions (Figure 5B,E,H) indicated the occurrence of CE reactions and the evolution of the Cu signal with increasing temperature. While the Cu signal in the RT map was localized only on the Cu_2Se NCs, an additional faint Cu signal was discriminated over the carbon film already at 350 °C. HRTEM characterization confirmed the transformation from hexagonal hcp CdSe NWs into the corresponding cubic fcc Cu_2Se (Figure 5C,F,I). In such a case, CdSe NWs at RT exhibit the main $\{0002\}$ and $\{11\bar{2}0\}$ lattice planes of an hcp structure in perpendicular vector orientation, as confirmed by Fourier analysis (FT inset of Figure 5C) compatible with the $[\bar{1}100]$ zone axis projection. At 350 °C, the NWs exhibited a cubic structure characterized by evident $\{11\bar{1}\}$ and $\{1\bar{1}1\}$ lattice planes forming an angle of 70° and pervasive $\{1\bar{1}1\}$ planar stacking faults crossing the lattice. The corresponding Fourier analysis, compatible with the $[011]$ zone axis projection of a fcc structure, revealed accordingly a strong linear streak consistent with this type of defective structure (FT inset of Figure 5F). Finally, at 400 °C, the totally exchanged NWs evidenced only lattice sets of cubic fcc $Cu_{2−x}Se$. In particular, Figure 5I and the FT inset display the $[011]$ HRTEM zone axis projection of an exchanged NW exhibiting the typical $\{11\bar{1}\}$ and $\{1\bar{1}1\}$ lattice planes of a fcc structure forming an angle of 70°, as depicted in the Fourier analysis.

Moreover, the use of few CdSe nanowires, surrounded by many Cu_2Se NCs, enabled us to observe the Cu CE fronts moving along the length of the wires, as shown in Figure S4, and revealed the two-dimensional diffusion of Cu species on the substrate over time. In regard to this, the EFTEM maps, acquired under different thermal conditions (Figure 5B,E,H) and normalized according to the method reported in ref 22, exhibited an evolution of the Cu signal with increasing temperature.

In Situ TEM Simultaneous Heating of Metal Cu Nanocrystals and CdSe Nanorods.

In order to confirm the role of the copper source in the CE reaction mechanism observed between Cu_2Se NCs and CdSe NRs, further experiments were performed using metal Cu NCs as copper donors. The concentration of Cu NCs was lowered with
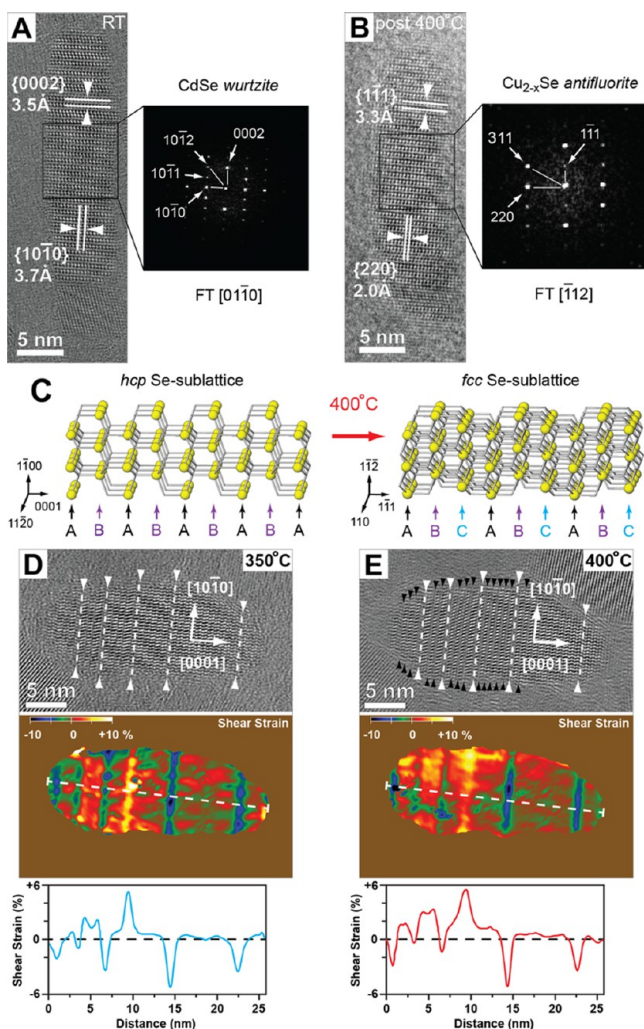

Figure 4. HRTEM investigation of a CdSe nanorod during thermally activated solid state CE. (A) CdSe nanorod at the preheating stage (RT), with a length of 34 nm and exhibiting wurtzite structure, with mutually perpendicular $\{0002\}$ and $\{10\bar{1}0\}$ lattice planes and with $[0002]$ and $[10\bar{1}2]$ crystal directions forming an angle of about 43° (FT inset). (B) After thermal activation of CE, the nanorod was slightly reduced in length (29 nm) due to the Se loss. The rod exhibited the cubic symmetry of the antifluorite structure of the $Cu_{2−x}Se$ phase with mutually perpendicular $\{1\bar{1}1\}$ and $\{220\}$ lattice planes and $[1\bar{1}1]$ and $[311]$ crystal directions forming an angle of about 58° (FT inset). Right panels of both (A) and (B) show the corresponding Fourier transforms, consistent with hexagonal $[01\bar{1}0]$ and cubic $[\bar{1}12]$ zone axes, respectively. (C) Structural sketch representing the NRs' hcp and fcc Se sublattices (yellow spheres) of wurtzite CdSe (preannealing) and cubic antifluorite Cu_2Se (postannealing). (D,E) HRTEM images with planar stacking faults (white and black arrows) and the corresponding shear strain maps of a nanorod at 350 and 400 °C with the integrated shear strain line profiles (white dotted lines).
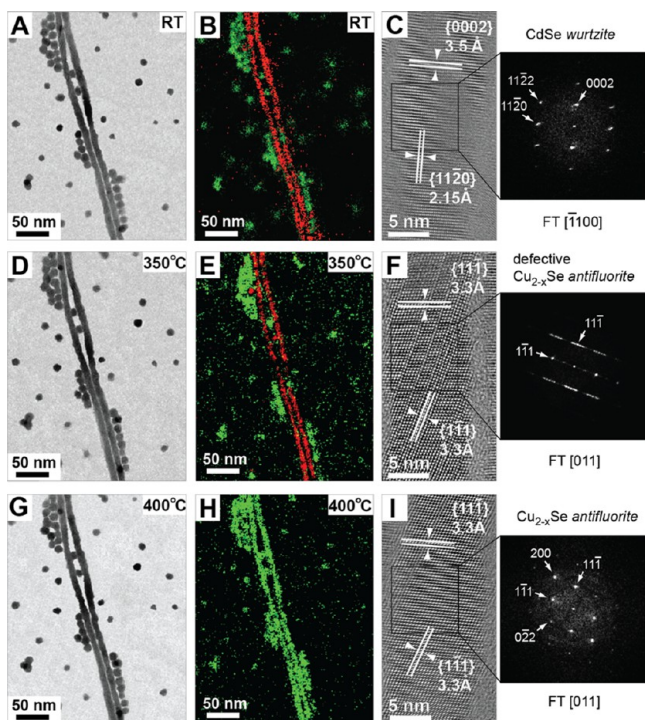
Figure 5. Sequence of elastic-filtered TEM, normalized EFTEM, and HRTEM imaging of $Cu_{2-x}Se$ NCs and CdSe nanowires. Imaging acquired at RT (A−C), intermediate temperature of 350 °C (D−F), and post-thermal treatment at 400 °C (G−I). The elastic-filtered EFTEM images (A,D,G) show no substantial shape changes during the thermal annealing. (B) Normalized EFTEM map at RT clearly displaying Cu (green) and Cd (red) localization in Cu_2Se NCs and CdSe nanowires, respectively. (C) HRTEM data of CdSe nanowires at RT reveal a hexagonal lattice (FFT inset). (E) Normalized EFTEM map at 350 °C clearly displays an increase of Cu signal on the C film between the NCs correlated to random diffusion of Cu species expelled from Cu_2Se NCs and migrating toward the Cu acceptor CdSe nanowire. (F) HRTEM data of incipient transformed CdSe nanowires into $Cu_{2-x}Se$ at 350 °C reveal a cubic lattice characterized by pervasive tacking faults, with a FFT (inset) compatible with the [011] zone axis of a fcc structure. (H) Normalized EFTEM mapping at post-400 °C annealing. Only the Cu signal was detected, while no signal from Cd was found. (I) HRTEM imaging of nanowires after thermal CE showing the only lattice sets of cubic antifluorite $Cu_{2-x}Se$, consistent with the [011] zone axis projection of the cubic structure (FFT inset).

Figure 6. EFTEM characterization of CdSe and Cu NCs before and after annealing at 400 °C. (A,B) Zero loss (ZL) image and Cu elemental map from CdSe rods in close proximity to Cu NCs before annealing. C,D) Same area after annealing at 400 °C showing the partial dissolution of the Cu NCs in the ZL image and the concomitant Cu incorporation in two of the rods in the Cu elemental map. (E) ZL image and (F) corresponding elemental map (Cu, green; Cd, red) showing examples of complete, partial, and no CE in the rods, depending on their location with respect to other rods and Cu source. (G) ZL image of nanorods (which had a CdSe composition before annealing) located more than 300 nm away from Cu source and (H) corresponding elemental map (Cu, green; Cd, red) after annealing at 400 °C, showing the complete exchange of the rods to $Cu_{2-x}Se$.

respect to the experiments involving Cu_2Se NCs in order to verify whether full or partial CE could still be observed by decreasing the net amount of copper available to the reaction. The results, summarized in Figures 6 and S5, indicate that CE takes place in the CdSe NRs, with the concomitant structural and chemical transformation to $Cu_{2-x}Se$. The CE was also found to be dependent on the local surface density and proximity of the Cu NCs deposited on the TEM substrate. The Cu NCs, visible as coarse cuboidal nanoparticles among the CdSe rods in Figure 6A,B, underwent partial dissolution during heating, and the released copper was engaged in CE with the adjacent CdSe NRs, as indicated in Figure 6C,D. The CE was always found to progress from the rods' end, along the c-axis (Figure S5B). In particular, detailed characterization by HRTEM revealed examples of both partially and fully structurally transformed and exchanged rods. In analogy with the previous experiments, as the CE reaction progressed, the same directionality was maintained between the exchanged and
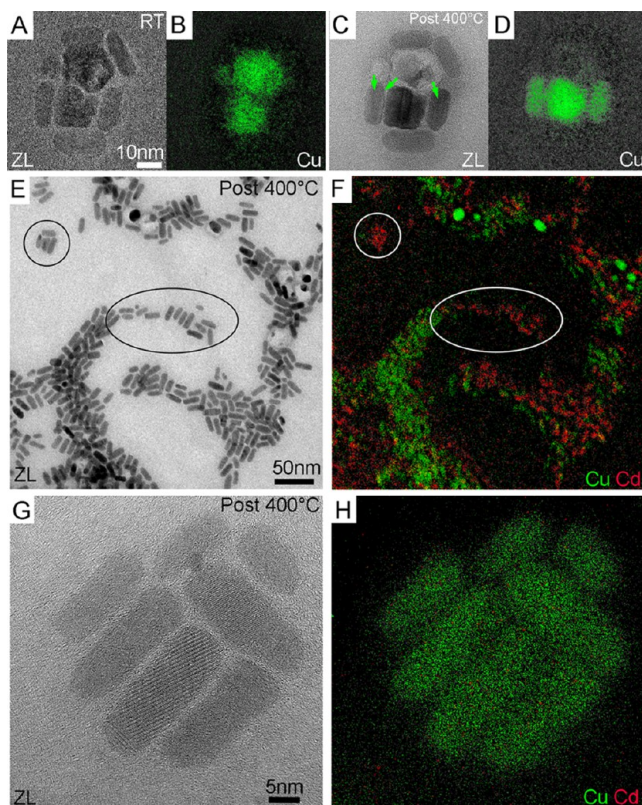
unexchanged parts of the NRs; that is, $[0001]_{hcp}$ was converted into $[111]_{fcc}$ (Figure S5), with an epitaxial interface between the exchanged and unexchanged parts of the rod and with the orientation relationship $\langle 0110 \rangle\{0001\}CdSe \| \langle 011 \rangle\{111\}$-$Cu_{2-x}Se$. This, along with the preferential shrinking also observed in the case of $Cu_2Se//CdSe$ CE reactions indicates that the c-axis of the nanorods offers a preferential direction of CE front in the CdSe lattice. The EFTEM images acquired after annealing at 400 °C for 90 min and displayed in Figure 6E,F also show that CdSe NRs in close proximity to the Cu NCs underwent CE, while other CdSe NRs that were isolated and flanked by other NRs underwent partial or no CE and retained most of the Cd in their structure, as confirmed by an EDX compositional analysis of individual NRs. This supports our hypothesis that the Cd expulsion from the rods is driven by copper in-diffusion and CE in the rods, rather than being only an annealing effect. In particular, Figure 6G,H shows that an isolated cluster of CdSe rods more than 300 nm away from the copper source (in such a case an array of Cu NCs) also underwent CE, confirming the very high mobility of the Cu species diffusing on the substrate at 400 °C. In order to

eliminate a possible electron beam effect during the CE in the presence of Cu NCs, solid-state CE annealing experiments were performed *ex situ* in a furnace under conditions similar to those in the TEM column: similar chemical CE and structural transformation were observed here, as well.

Our experiments indicate that the free Cu species, once expelled from their original and local source, reach the acceptor particles and there give rise to a thermally activated CE reaction. One potential mechanism for distributing such free Cu species over the CdSe NRs/NWs (and therefore enable CE) is *via* vapor phase diffusion. In such case, the expelled Cu should recondense from the vapor phase on the hot TEM grid. However, this appears unlikely for a series of reasons. First, the sample was heated under high and dynamic vacuum and with a cryogenic trap located in close proximity to the sample that should promptly adsorb any chemical released by the sample by sublimation. Second, in the unlikely event of recondensation of copper from the vapor phase, then under the high-vacuum conditions in which the experiment is performed, such Cu should have recondensed uniformly and isotropically over the whole substrate and enabled CE also on NRs/NWs that were far from any Cu$_2$Se/Cu NC. This is contrary to our observation of a locality effect in CE, as more distal NRs/NWs were less affected by CE or were not exchanged at all. Finally, if Cu was able to recondense on the substrate, a similar fate should have occurred to the sublimated Cd and (in part) Se species. Then, we should have been able to map the presence of Cd and Se in regions that were not initially occupied by CdSe NRs/NWs.

A more plausible scenario is that the copper species expelled by the Cu$_2$Se/Cu NCs diffuse over the amorphous substrate that constitutes the mechanical support for the nanostructures in the TEM grid. Two pieces of experimental evidence support this second scenario. First, our normalization approach to the whole set of EFTEM images collected at the different samples' temperatures allowed us to make them coherent in terms of signal-to-background discrimination, permitting then to attribute the increase in the Cu signal (observed on the amorphous substrate already at 350 °C) to the out-diffusion of the Cu species expelled from Cu$_2$Se NCs, which could then reach the CdSe particles, as expected for a simple thermal diffusion process over an amorphous substrate.[23] Second, there is a proximity effect on Cu depletion of the NCs acting as copper sources, which is strongly in favor of a surface diffusion process. After annealing, the chemical composition of the original Cu$_2$Se NCs, acquired *via* STEM-EDX, showed a variation in Cu depletion of the NCs that depended on their distance (D) from the CdSe NWs: the composition of the NCs ranged from Cu$_{1.83}$Se (when D < 100 nm) to Cu$_{1.92}$Se (when 100 nm < D < 500 nm). An analogous effect was observed also when Cu NCs were used instead of Cu$_2$Se as local sources of copper for the *in situ* CE reaction. In this case, the Cu content in the partially or fully exchanged CdSe NRs markedly depended on the proximity of the copper source, the Cu NCs, and the presence of other Cu scavengers on the substrate along the diffusion path (other CdSe NRs), ranging from Cu$_{2.1}$Se in close proximity to the cluster of Cu NCs to Cu$_{1.5}$Se further away from the copper source. Finally, as expected, we observed that—once the activation energy to start the CE reaction had been reached by crossing the threshold temperature—its kinetics, that is, the rate of CE reaction, increased with increasing temperature. Besides, we also noticed that such a rate depends on the type of cation donor species. Even if elucidating the reasons for these differences is beyond the main aim of this paper, further

experimental studies and theoretical simulations are currently being performed in our groups to shed more light on such issue.

Since the exchange was observed not only on CdSe NCs directly in contact with Cu$_2$Se NCs but also on those several nanometers apart, this leads us to discuss a second and fundamental point, the latter concerning the migration mechanism followed by the copper expelled by the NCs acting as its sources: which was its oxidation state during the diffusion on the substrate? In this case, it would be unlikely for the Cu species to leave the Cu$_2$Se NCs as charged ions and thermally diffuse on the substrate. A more plausible explanation is that thermal annealing causes a release of Cu species from the Cu$_2$Se NCs as zerovalent (Cu^0) atoms that can move randomly on the amorphous carbon film, similarly to the two-dimensional diffusion process of metallic atom species over a substrate.[23,24] Also, it is unlikely that the amorphous nature of the carbon film could allow the expelled Cu^0 atoms to follow any favored migration paths and therefore to self-organize into clusters along certain preferential directions. Since both species involved in the exchange (Cu and Cd) exist as cations only when they are in the NCs, and as the NCs evolve from CdSe to Cu$_{1.96}$Se, this chemical and structural transformation can be considered as a CE reaction mediated by an intermediate step with migrating Cu^0 free atoms. Furthermore, this Cu^0-mediated process was corroborated by the thermally driven CE reaction occurring in CdSe when metallic copper NCs instead of Cu$_2$Se NCs were used as Cu donor nanospecies.

The cation exchange reactions observed in all the experiments were triggered solely by annealing. We found indeed that the thermal CE between CdSe and Cu$_2$Se took place also in those areas that were never directly exposed to the electron beam irradiation, occurring even in samples heated at 400 °C in the TEM with the beam blanked (Figure S6), as well as in the CdSe rods in the presence of Cu NCs on a TEM grid heated *ex situ*. We additionally tested a Si$_3$N$_4$ support as a different type of amorphous substrate, and also in this case CE took place at 400 °C (Figure S7), indicating that the unreactive chemical nature of the substrates does not affect the migration of the copper and the consequent *in situ* CE reaction. We finally carried out additional experiments outside the electron microscope, by annealing similar CdSe and Cu$_2$Se samples in the high-vacuum prechamber of an X-ray photoelectron spectrometer (XPS), followed by their immediate XPS analysis at different temperatures with no air exposure (Figure S8). These experiments confirmed our previous findings and ruled out any role of electron irradiation in the CE reactions.

CONCLUSIONS

We showed how thermally activated cation exchange reactions involving different kinds of NCs deposited on the same substrate can occur and be studied by an *in situ* TEM approach. Besides, we showed that such CE reactions, when performed in a solid state, took tens of minutes to be completed: their kinetics is much slower than in the liquid phase, where they often take only a fraction of a second to reach completion. This calls for further investigations aimed at understanding whether the observed phenomena can take place even when both the donor and acceptor species (Cu$_2$Se/Cu and CdSe NCS, respectively) are assembled as extended aggregates and, consequently, how the NC aggregation state (*i.e.*, the possible degree of order/assembly of the NCs) could influence the thermally driven solid-state CE reaction. Our *in situ* TEM

approach to the study of the solid-state exchange reactions could then open interesting perspectives in identifying the intermediate states of such transformations and could be applicable to many other combinations of materials. It could additionally pave the way to methods for the modification of chemical composition, crystal structure, and physicochemical properties of materials at a local scale.

MATERIALS AND METHODS

Synthesis of NCs. Syntheses were carried out following standard published procedures. All details on synthesis and processing of the NCs are reported in the Supporting Information.

***In Situ* TEM Thermal Heating Experiments.** *In situ* thermal heating experiments were performed within the TEM column, that is, under high-vacuum conditions (pressure $P \sim 1.5 \times 10^{-5}$ Pa), using a dedicated single tilt heating holder capable of reaching a maximum temperature of 800 °C. In those experiments that required the concomitant presence of both copper cation donor (Cu_2Se NCs or Cu NCs) and acceptor (CdSe rods or CdSe wires) species on the ultrathin carbon-coated gold TEM grid, these species were not deposited on the grid from a common solution. Instead, two sequential depositions of the respective solutions were made on the TEM grid. This procedure was followed in order to minimize as much as possible any cation exchange reaction already in the solution phase, that is, prior to deposition and annealing.

Before the *in situ* experiments were performed, these samples were cleaned with ethanol and heated at 130 °C in a pumping station ($P \sim 10^{-3}–10^{-4}$ Pa) in order to eliminate the residuals of excess surfactants. Note that this treatment should not remove quantitatively the surfactants bound to the surface of the NCs. *In situ* TEM thermal treatment of all samples was carried out according to a common protocol: the system was initially heated from room temperature to 300 °C at a heating rate of 5 °C min^{-1} and afterward up to a reaction temperature of 400 °C at a heating rate of 2.5 °C min^{-1}. This helped to minimize thermal drift and enabled monitoring the exchange reaction over time after its thermal activation.

Transmission Electron Microscopy Characterizations. *HR-EELS Analysis.* This was performed in STEM mode with a FEI Titan 80-300 Cube with double spherical aberration correction of both condenser and objective lens, working at an accelerating voltage of 300 kV and equipped with an ultra-bright-field emission gun (XFEG), an electron monochromator, and a GIF Quantum ERS energy spectrometer, with a final energy resolution of 0.10 eV (at KAUST, Thuwal, Saudi Arabia) for the Cu_2Se NCs and of 0.07 eV (at McMaster University, Hamilton, Ontario, Canada) for the $Cu_{2-x}Se$ NCs. In both experiments, HR-EELS analysis was carried out in single range mode, focusing on the low loss energy region from 0 to 20 eV and with an exposure time of 1 ms per pixel on an area of 0.1 μm^2, yielding a total exposure time of 75 s per investigated region. Detailed chemical analysis *via* EELS was carried out in TEM and STEM mode (spectrum imaging) using a FEI Tecnai G2 F20 microscope, working at 200 kV, equipped with field emission electron source, a GIF Quantum ER energy filter, and a Gatan K2-Summit direct detection camera (at Gatan Inc., Pleasanton, CA, USA). The EELS spectra were acquired from 300 to 2300 eV energy range in order to detect any fine variation in the energy profile of the Cd M-edge (404 eV), Cu L-edge (931 eV), and Se L-edge (1436 eV), with an exposure time of 8 ms per pixel on an area of 0.25 μm^2, yielding a total exposure time of a few minutes per investigated region.

HRTEM, HAADF-STEM, STEM-EDX, and EFTEM Analysis. These measurements were performed by a JEOL JEM-2200FS microscope, working at 200 kV, equipped with a Schottky electron source, a CEOS spherical aberration corrector of the objective lens, an in-column Omega energy filter, and a Gatan US1000 CCD camera (at Istituto Italiano di Tecnologia, Genova, Italy). Spatially resolved chemical analysis of NCs was performed in STEM mode *via* EDX using a Bruker Quantax 400 XFlash 6T silicon drift detector (SDD) with an area of 60 mm^2. STEM-EDX analyses were carried out at room temperature before and after the heating experiments in order to avoid

saturation of the SDD detector due to infrared thermal emission of the heated TEM holder. Elemental maps *via* EFTEM imaging were acquired using a contrast aperture of about 10 mrad to reduce aberrations, mostly chromatic, and using the three-window method (one post- and two pre-edge) to extract the background. The elastic (zero loss) image was acquired as reference with a 10 eV wide energy slit; then, elemental maps using Cu L-edge (931 eV) and Cd M-edge (404 eV) were acquired on the same area of zero loss with energy slits of 50 and 30 eV, respectively, and normalized according to the method reported in ref 22.

Electron Diffraction Analysis. Selected area electron diffraction patterns (SAEDPs) were acquired using a FEI Tecnai G2 F20 microscope working at 200 kV, equipped with a Schottky electron source and Gatan US1000 CCD camera with a high-sensitive thick scintillator (at Istituto Italiano di Tecnologia, Genova, Italy). Cubic $Cu_{2-x}Se$ and hexagonal CdSe SAEDPs were indexed using ICSD card no. 67050 and no. 41491, respectively.

Strain Field Analysis. The strain field was measured using the peak pairs analysis[25] starting from the HRTEM images. Strain maps, displaying the in-plane components of the symmetric strain tensors, were generated by considering the deformation stored in the rod lattice. Within the PPA method, the structural displacements, u_{ij} of the atomic columns were used to calculate the in-plane shear strain tensor, $\varepsilon_{xy} = \frac{1}{2}\left(\frac{\partial u_x}{\partial y} + \frac{\partial u_y}{\partial x}\right)$, considering as the lattice basis vectors the 0002 and 10$\bar{1}$0 "structural reflections". The coordinates of u_{ij} displacements were chosen such that the x-axis was parallel to the [0001] crystal axis, corresponding to the rod elongation, as well.

DFT Simulations of the Low Loss EEL Spectrum. The low loss EEL spectrum was modeled *via* DFT using the random phase approximation (Vienna Ab Initio Simulation Package).[26] The projector-augmented wave method (plane wave cutoff energy of 800 eV) was employed, together with the generalized gradient approximation for the exchange-correlation functional in the Perdew–Burke–Ernzerhof flavor.[27] Both Cu_2Se and $Cu_{2-x}Se$ were optimized up to an energy convergence of 10^{-5} eV and a force convergence of 4 meV/Å. Monkhorst–Pack k-meshes of $8 \times 8 \times 8$ (structure relaxation) and $16 \times 16 \times 16$ (optical calculations) points were used for Brillouin zone integrations. The DFT simulations were carried out considering a stoichiometric Cu_2Se crystal and a virtual Cu-depleted $Cu_{2-x}Se$ crystal, both with fcc antifluorite structure and a $\sqrt{2} \times \sqrt{2} \times 1$ unit cell size. The Cu-depleted $Cu_{2-x}Se$ crystal was obtained by removing one atom of Cu from the total 16 Cu and 8 Se atoms. This removal, due to the cubic symmetry of antifluorite phase, generates 6.25% vacancies of Cu in the crystal lattice corresponding to $Cu_{1.88}Se$ stoichiometry (which is a close estimate of the vacancy concentration that was measured experimentally). The imaginary part of the frequency-dependent dielectric tensor was obtained from the first-principles eigenstates and afterward the real part by means of the Kramers–Kronig relations. Thus, the EEL spectrum was determined in the random phase approximation.

ASSOCIATED CONTENT

Ⓢ Supporting Information

The Supporting Information is available free of charge on the ACS Publications website at DOI: 10.1021/acsnano.5b07219.

> Details on the chemical synthesis of nanocrystals; structural characterization of Cu_2Se nanocrystals *via* electron diffraction at pre- and post-heating conditions; element quantification of $Cu_{2-x}Se$ nanocrystals *via* EELS post-heating conditions; HR-EELS analysis; structural and thermodynamic details on the chemical and crystal structure transformation of nanorods from wurtzite CdSe to antifluorite $Cu_{2-x}Se$; annealing experiment on CdSe nanorods alone; normalized element mapping *via* EFTEM of CdSe nanowires and Cu_2Se nanocrystals; *in situ* TEM simultaneous heating of metal Cu nanocrystals

and CdSe nanorods; HRTEM images of partially and completely exchanged CdSe nanorods; element mapping *via* EFTEM of CdSe nanowires and Cu$_2$Se nanocrystals annealed in beam-blanked conditions; element mapping *via* normalized EFTEM of CdSe nanorods and Cu$_2$Se nanocrystals on a Si$_3$N$_4$ TEM grid; and X-ray photoelectron spectroscopy characterization (PDF)

AUTHOR INFORMATION

Corresponding Authors
*E-mail: liberato.manna@iit.it.
*E-mail: andrea.falqui@kaust.edu.sa.

Author Contributions
△A.C. and A.G. contributed equally to this work.

Notes
The authors declare no competing financial interest.

REFERENCES

(1) Sitt, A.; Hadar, I.; Banin, U. Band-gap engineering, optoelectronic properties and applications of colloidal heterostructured semiconductor nanorods. *Nano Today* 2013, 8, 494−513.

(2) Talapin, D. V.; Lee, J. S.; Kovalenko, M. V.; Shevchenko, E. V. Prospects of Colloidal Nanocrystals for Electronic and Optoelectronic Applications. *Chem. Rev.* 2010, 110, 389−458.

(3) Son, D. H.; Hughes, S. M.; Yin, Y. D.; Alivisatos, A. P. Cation exchange reactions in ionic nanocrystals. *Science* 2004, 306, 1009−1012.

(4) Rivest, J. B.; Jain, P. K. Cation exchange on the nanoscale: an emerging technique for new material synthesis, device fabrication, and chemical sensing. *Chem. Soc. Rev.* 2013, 42, 89−96.

(5) Beberwyck, B. J.; Surendranath, Y.; Alivisatos, A. P. Cation Exchange: A Versatile Tool for Nanomaterials Synthesis. *J. Phys. Chem. C* 2013, 117, 19759−19770.

(6) Gupta, S.; Kershaw, S. V.; Rogach, A. L. 25th Anniversary Article: Ion Exchange in Colloidal Nanocrystals. *Adv. Mater.* 2013, 25, 6923−6944.

(7) De Trizio, L.; De Donato, F.; Casu, A.; Genovese, A.; Falqui, A.; Manna, L. Colloidal CdSe/Cu$_3$P/CdSe Nanocrystal Heterostructures and Their Evolution upon Thermal Annealing. *ACS Nano* 2013, 7, 3997−4005.

(8) Yalcin, A. O.; Fan, Z.; Goris, B.; Li, W. F.; Koster, R. S.; Fang, C. M.; Van Blaaderen, A.; Casavola, M.; Tichelaar, F. D.; Bals, S.; Van Tendeloo, G.; Vlugt, T. J. H.; Vanmaekelbergh, D.; Zandbergen, H. W.; Van Huis, M. A. Atomic Resolution Monitoring of Cation Exchange in CdSe-PbSe Heteronanocrystals during Epitaxial Solid−Solid−Vapor Growth. *Nano Lett.* 2014, 14, 3661−3667.

(9) Figuerola, A.; van Huis, M.; Zanella, M.; Genovese, A.; Marras, S.; Falqui, A.; Zandbergen, H. W.; Cingolani, R.; Manna, L. Epitaxial CdSe-Au Nanocrystal Heterostructures by Thermal Annealing. *Nano Lett.* 2010, 10, 3028−3036.

(10) Comin, A.; Manna, L. New materials for tunable plasmonic colloidal nanocrystals. *Chem. Soc. Rev.* 2014, 43, 3957−3975.

(11) Bekenstein, Y.; Vinokurov, K.; Keren-Zur, S.; Hadar, I.; Schilt, Y.; Raviv, U.; Millo, O.; Banin, U. Thermal Doping by Vacancy Formation in Copper Sulfide Nanocrystal Arrays. *Nano Lett.* 2014, 14, 1349−1353.

(12) Dorfs, D.; Härtling, T.; Miszta, K.; Bigall, N. C.; Kim, M. R.; Genovese, A.; Falqui, A.; Povia, M.; Manna, L. Reversible Tunability of the Near-Infrared Valence Band Plasmon Resonance in Cu$_{2-x}$Se Nanocrystals. *J. Am. Chem. Soc.* 2011, 133, 11175−11180.

(13) Luther, J. M.; Zheng, H. M.; Sadtler, B.; Alivisatos, A. P. Synthesis of PbS Nanorods and Other Ionic Nanocrystals of Complex Morphology by Sequential Cation Exchange Reactions. *J. Am. Chem. Soc.* 2009, 131, 16851−16857.

(14) Kriegel, I.; Jiang, C.; Rodríguez-Fernández, J.; Schaller, R. D.; Talapin, D. V.; Da Como, E.; Feldmann, J. Tuning the Excitonic and Plasmonic Properties of Copper Chalcogenide Nanocrystals. *J. Am. Chem. Soc.* 2012, 134, 1583−1590.

(15) El Akkad, F.; Mansour, B.; Hendeya, T. Electrical and Thermoelectric Properties of Cu$_2$Se and Cu$_2$S. *Mater. Res. Bull.* 1981, 16, 535−539.

(16) Miller, T. A.; Wittenberg, J. S.; Wen, H.; Connor, S.; Cui, Y.; Lindenberg, A. M. The Mechanism of Ultrafast Structural Switching in Superionic Copper (I) Sulphide Nanocrystals. *Nat. Commun.* 2013, 4, 1369.

(17) Balapanov, M. K.; Ishembetov, R. K.; Yulaeva, Y. K.; Yakshibaev, R. A. Thermodynamic Properties of Solid Solutions of Superionic Copper, Silver, and Lithium Chalcogenides. *Russ. J. Electrochem.* 2011, 47, 1337−1342.

(18) Glazov, V. M.; Pashinkin, A. S.; Fedorov, V. A. Phase Equilibria in the Cu-Se System. *Inorg. Mater.* 2000, 36, 641−652.

(19) Heyding, R. D.; Murray, R. M. The Crystal Structures of Cu$_{1.8}$Se, Cu$_3$Se$_2$, α- and γ-CuSe, CuSe$_2$, and CuSe$_2$ II. *Can. J. Chem.* 1976, 54, 841−848.

(20) Liu, H.; Shi, X.; Xu, F.; Zhang, L.; Zhang, W.; Chen, L.; Li, Q.; Uher, C.; Day, T.; Snyder, G. J. Copper Ion Liquid-like Thermoelectrics. *Nat. Mater.* 2012, 11, 422−425.

(21) Balitskii, O. A.; Sytnyk, M.; Stangl, J.; Primetzhofer, D.; Groiss, H.; Heiss, W. Tuning the Localized Surface Plasmon Resonance in Cu$_{2-x}$Se Nanocrystals by Postsynthetic Ligand Exchange. *ACS Appl. Mater. Interfaces* 2014, 6, 17770−17775.

(22) Casu, A.; Genovese, A.; Di Benedetto, C.; Lentijo-Mozo, S.; Sogne, E.; Zuddas, E.; Falqui, A. A Facile Method to Compare EFTEM Maps Obtained from Materials Changing Composition Over Time. *Microsc. Res. Tech.* 2015, 78, 1090−1097.

(23) Egelhoff, W. F.; Tibbetts, G. G. Growth of Copper, Nickel, and Palladium Films on Graphite and Amorphous Carbon. *Phys. Rev. B: Condens. Matter Mater. Phys.* 1979, 19, 5028−5035.

(24) Gan, Y. J.; Sun, L. T.; Banhart, F. One- and Two-dimensional Diffusion of Metal Atoms in Graphene. *Small* 2008, 4, 587−591.

(25) Galindo, P. L.; Kret, S.; Sanchez, A. M.; Laval, J. Y.; Yáñez, A.; Pizarro, J.; Guerrero, E.; Ben, T.; Molina, S. I. The Peak Pairs Algorithm for Strain Mapping from HRTEM Images. *Ultramicroscopy* 2007, 107, 1186−1193.

(26) Kresse, G.; Furthmuller, J. Efficient Iterative Schemes for Ab Initio Total-energy Calculations Using a Plane-wave Basis Set. *Phys. Rev. B: Condens. Matter Mater. Phys.* 1996, 54, 11169−11186.

(27) Perdew, J. P.; Burke, K.; Ernzerhof, M. Generalized Gradient Approximation Made Simple. *Phys. Rev. Lett.* 1996, 77, 3865−3868.

(28) Gulay, L.; Daszkiewicz, M.; Strok, O.; Pietraszko, A. Crystal Structure of Cu$_2$Se. *Chem. Mater. Alloys* 2011, 4, 200−205.